J. Fluid Mech. (1998), *vol.* 375, *pp.* 363–381. Printed in the United Kingdom

© 1998 Cambridge University Press

Direct droplet production from a liquid film: a new gas-assisted atomization mechanism

By HERMAN E. SNYDER AND ROLF D. REITZ†
Mechanical Engineering Department, 1500 Engineering Drive, University of Wisconsin-Madison, WI 52706, USA

(Received 30 June 1997 and in revised form 1 July 1998)

X-ray lithography and micro-machining have been used to study gas-assisted liquid atomization in which a liquid film was impinged by a large number of sonic micro-gas jets. Three distinct breakup regimes were demonstrated. Two of these regimes share characteristics with previously observed atomization processes: a bubble bursting at a free surface (Newitt *et al.* 1954; Boulton-Stone & Blake 1993) and liquid sheet disintegration in a high gas/liquid relative velocity environment (Dombrowski & Johns 1963). The present work shows that suitable control of the gas/liquid interface creates a third regime, a new primary atomization mechanism, in which single liquid droplets are ejected directly from the liquid film without experiencing an intermediate ligament formation stage. The interaction produces a stretched liquid sheet directly above each gas orifice. This effectively pre-films the liquid prior to its breakup. Following this, surface tension contracts the stretched film of liquid into a sphere which subsequently detaches from the liquid sheet and is entrained by the gas jet that momentarily pierces the film. After droplet ejection, the stretched liquid film collapses, covering the gas orifice, and the process repeats. This new mechanism is capable of the efficient creation of finely atomized sprays at low droplet ejection velocities (e.g. 20 μm Sauter mean diameter methanol sprays using air at 239 kPa, with air-to-liquid mass ratios below 1.0, and droplet velocities lower than 2.0 m s^{-1}). Independent control of the gas and the liquid flows allows the droplet creation process to be effectively de-coupled from the initial droplet momentum, a characteristic not observed with standard gas-assisted atomization mechanisms.

1. Introduction

A common method of liquid atomization involves the conversion of a liquid sheet into a dispersed field of discrete droplets in a gaseous medium. The sheet breakup mechanism was studied by Dombrowski & Johns (1963) who identified a two-part process. First, the sheet was segmented by those surface instabilities with the fastest growing wavenumber and subsequently formed liquid ligaments or cylinders. The ligaments further disintegrated into droplets due to capillary instabilities. For a particular liquid and ambient gas environment the relative gas-to-liquid velocity and the sheet thickness control the droplet size produced by this primary atomization process.

Frasier, Dombrowski & Routley (1963) investigated the impact of sheet thickness on the resulting droplet size when the liquid sheet was impinged by a normal gas flow. The spray was characterized by the Sauter mean diameter (SMD $= d_{32} = \sum N_i D_i^3 / \sum N_i D_i^2$)

† Author to whom correspondence should be addressed.

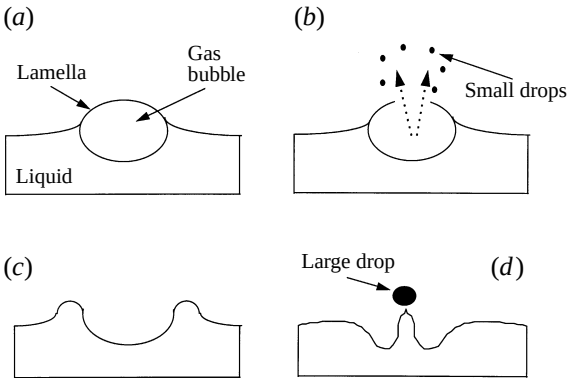

FIGURE 1. Bubble bursting mechanism, from Newitt *et al.* (1954).

which was found to be proportional to the liquid sheet thickness, $t^{0.5}$. Lefebvre (1989) reported a similar dependence, SMD $\propto t^{0.4}$, when both sides of the liquid sheet were exposed to parallel flows of high-speed gas. For both geometries, reducing the characteristic liquid length scale proved to be advantageous for the production of tiny liquid droplets.

One application of this theory can be seen in the production of small-diameter droplets from a bursting gas bubble at a liquid free surface, discussed by Newitt, Dombrowski & Knelman (1954). The authors reported two distinct mechanisms for liquid droplet production due to the bursting at the surface of 3.1 to 5.3 mm diameter air bubbles in a water bath, as outlined in figure 1. The two paths for droplet creation shown in the figure combined to produce a bimodal droplet size distribution with separate clusters of 'large'- and 'small'-diameter droplets. The interaction of the gas bubble with the free surface created a dome-shaped liquid film or lamella protruding from the surface, figure 1(*a*). The stretched liquid layer eventually ruptures near the top of the dome and the retracting liquid film is broken apart by the escaping gas from within the bubble, figure 1(*b*).

The breakage of the encapsulating dome lamella leaves behind an unstable free surface with a bubble 'crater' surrounded by liquid at the higher potential energy of the original surface, figure 1(*c*). The filling of this depression is augmented by a series of standing waves produced from the inertia of the bursting lamella. The rapid liquid inflow into the depression creates a standing liquid jet at the crater centre which breaks into droplets via capillary instabilities, i.e. the Rayleigh breakup mechanism, figure 1(*d*).

The authors reported SMD values from 18–33 μm for the small-droplet cluster and 610–1000 μm for the large-diameter group with the number of small droplets produced being greater than the number of large droplets by approximately an order of magnitude. However, given the d^3 dependence of the liquid volume, the majority of the mass in droplet formed is contained in the large droplets produced by the jet breakup. This fact explains why several studies have focused on the jet aspect of the process, such as the numerical investigation by Boulton-Stone & Blake (1993), while droplet production from the lamella bursting is not considered.

The formation of the lamella dome at the free surface provides a thin film for the creation of small droplets, as shown by Newitt *et al.* (1954). By forcing the liquid to take this shape, an aerodynamic 'prefilmer' is created which evidently performs the same function as a liquid spreading surface on a prefilming air-blast atomizer (Lefebvre

1989). The liquid is conditioned to minimize its characteristic length scale (thickness) prior to being fragmented by the relative gas/liquid velocity. In the bursting bubble example, a high relative velocity is provided by the escaping gas from within the bubble.

While a bubble bursting at a free surface exhibits the ability to produce droplets well below 50 μm in diameter, the majority of the liquid mass which is atomized is captured by the larger droplet size cluster. Therefore a method of creating a liquid stretching and rupture process similar to the lamella disintegration process, but without the jetting process, would provide for the efficient production of small droplets.

The present work outlines the application of unique micro-machining techniques to a liquid film breakup process which provides control of the liquid/gas interface on the micron size scale. As a result of this work, a new regime for efficient droplet production from a liquid film was observed in which the intermediate ligament production stage of the Dombrowski & Johns model is eliminated.

2. Experiment

The experimental portion of this work encompassed three distinct areas: (i) the production of a micro-machined membrane to provide a field of atomizing gas jets, (ii) the design of a droplet generator, and (iii) high-speed photography and the measurement of the resulting droplet sizes and velocities.

Toroidal shaped membranes containing 4200 gas flow orifices, shown in figure 2, were constructed using a combination of X-ray lithography and nickel electro-deposition, with the process details outlined by Snyder (1997). One set of membranes contained an array of $\phi = 7$ μm diameter gas flow orifices with length-to-diameter (L/D) ratios of 12:1 or 23:1. Within each membrane the orifices were arranged in a pattern of 35 concentric circles; each circle contained 120 orifices and adjacent circles were offset 1.5° circumferentially. This spacing was chosen to prevent adjacent gas jets from coalescing within the liquid film.

The use of X-rays during the lithographic portion of the construction process provided sub-micron feature control with large part aspect ratios while maintaining orthogonal sidewalls, characteristics unobtainable using standard UV processes. The exposed photoreactive polymer was dissolved away leaving behind a 'mould' in which the final nickel part is electrodeposited. Figure 3(*a*) displays a scanning electron microscope image of a single 7 μm diameter polymer cylinder. The nickel is deposited around the cylinder and then the polymer is removed, leaving the highly cylindrical, square-edged 7 μm diameter flow orifice up to 160 μm deep, as shown in figure 3(*b*).

A third membrane was constructed with an array of 50 μm diameter holes and with $L/D = 3.5$ to evaluate the impact of flow orifice diameter on the atomization process. This membrane contained 205 orifices along two concentric circles with inter-hole spacings of 444 and 455 μm.

A comparison of atomizer performance between the X-ray lithographic produced membranes and a commercial electroplated product was reported by Snyder (1997), and highlighted the need for well-defined micron-sized flow passages.

The micro-machined membranes were mounted in a droplet generator as shown in figure 4. Pressurized gas was supplied to the plenum chamber on one side of the membrane and driven through the 7 μm (or 50 μm) diameter orifices, creating a field of discharging gas jets on the opposite side of the membrane at ambient pressure. The liquid is delivered to the centre of the membrane and allowed to film over its top surface. The gas and liquid flow rates were measured using Gilmount calibrated

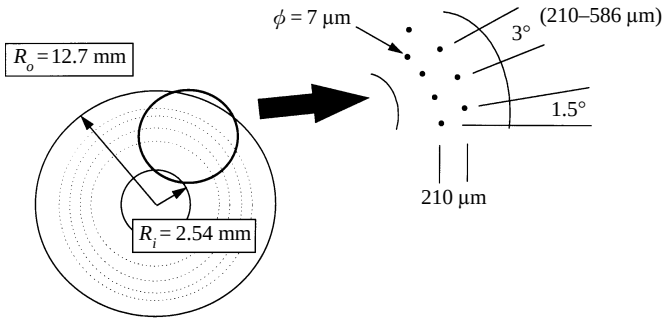

FIGURE 2. Micro-machined 7 μm orifice pattern.

(*a*)

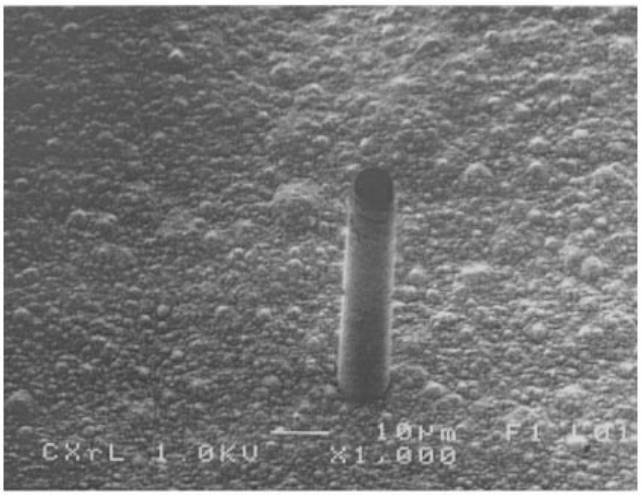

(*b*)

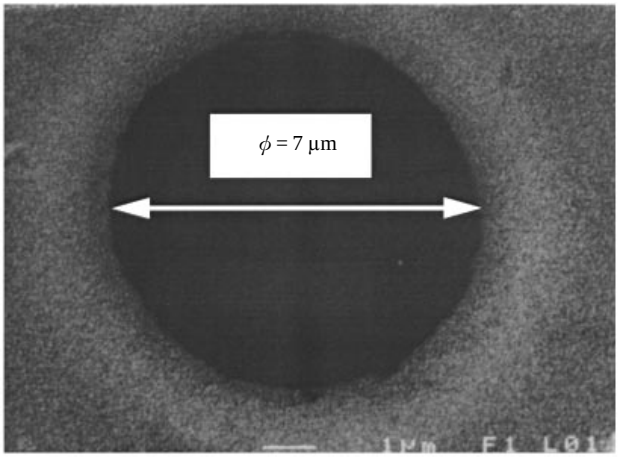

FIGURE 3. SEM photograph showing (*a*) polymer cylinder (orifice mould), and (*b*) flow orifice (end view).

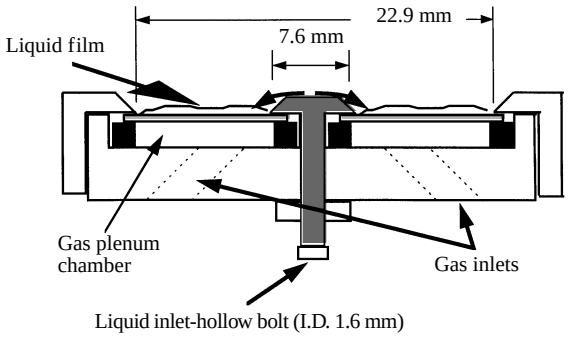

FIGURE 4. Droplet generator.

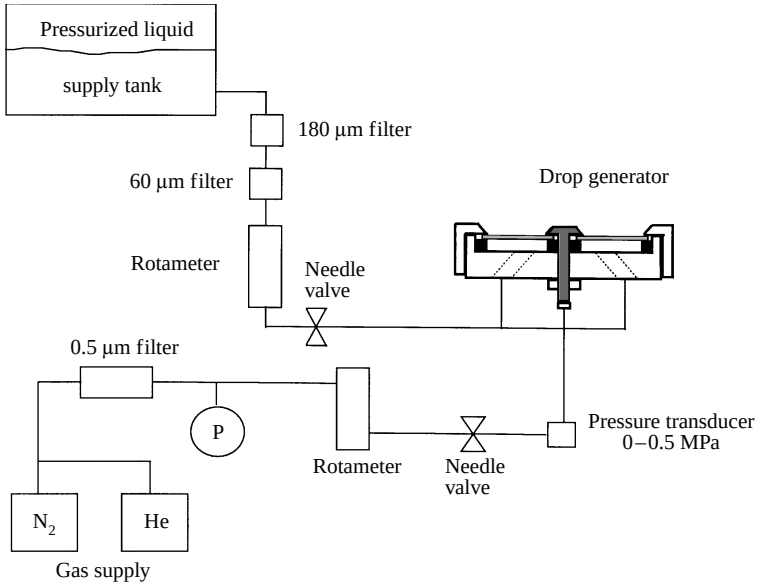

FIGURE 5. Schematic diagram of atomizer gas and liquid supply.

rotameters and analysis software with $\pm 2\%$ accuracy. A diagram showing the layout of the liquid and gas supply details is given in figure 5.

The effective thickness of the liquid film at the point of gas jet interaction is a function of the liquid and gas flow rates as well as the shape of the membrane surface. The two 7 μm orifice diameter membranes were 84 and 160 μm thick and exhibited some deflection from a flat plane when pressurized, as shown in figure 6 for 239 and 377 kPa. The thin ($L = 84$ μm, $L/D = 12$) foil produced a deflection greater than 200 μm at the centre of the exposed membrane annulus, located 3.8 mm from the inner restraint of the holding fixture, while the thick membrane ($L = 160$ μm) yielded a maximum deflection of approximately 60 μm. The reduced surface deflection improved the liquid film thickness uniformity for the $L/D = 23$ membrane.

The droplet sizes and velocities were measured at a location 12.7 mm above the droplet generator using an Aerometrics 1-D PDPA, DSA model with details of the instrument configuration provided in Snyder (1997).

Photographic techniques were employed to examine the near-surface structure of the micro-gas jet/liquid film interactions and yielded qualitative information on the mechanisms of droplet creation. The optical system, shown in figure 7, used a Questar

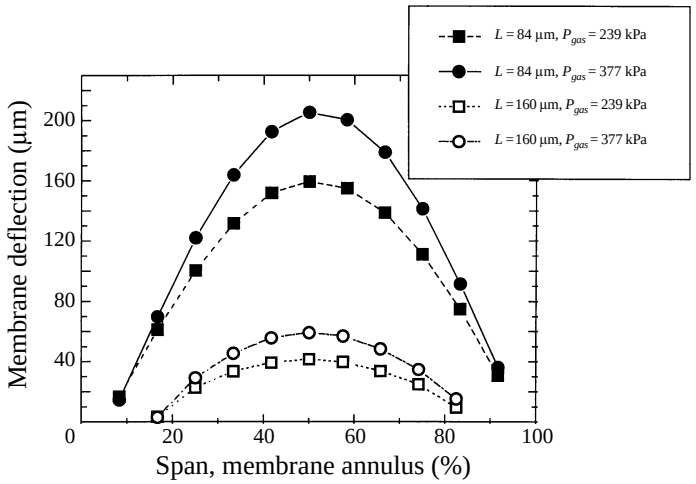

FIGURE 6. Membrane deflection.

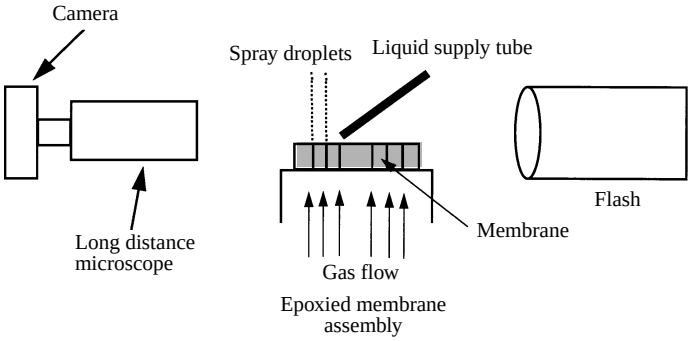

FIGURE 7. Photographic configuration.

QM-100 long distance microscope to provide high magnification and either 35 mm film or a Kodak HS4540 digital camera to provide high-speed movies (40 500 f.p.s.). The spray field was illuminated with an EG & G Micro-flash unit (0.5 µs duration) when using 35 mm film, and a 500 W flood lamp when using the Kodak digital camera. The system resolution using Kodak Technical Pan film was found to be approximately 3 µm. Selected membranes with 7 and 50 µm diameter orifices were epoxied to a flat fixture to provide orthogonal optical access to the top of the membrane. The liquid was directed to a limited portion of the top surface through a hypodermic tube. This geometry allowed for the qualitative identification of distinct regimes of droplet production. Various liquids were studied including water, methanol, diesel fuel and other hydrocarbon fuels (Snyder 1997). Only the methanol results are discussed here.

3. Results

3.1. *Gas flow through micro-orifices*

Examination of the gas flow characteristics required consideration of the Reynolds number, discharge coefficient, and entrance length for micro-orifices. The gas flow discharge coefficients for the micro-orifice membranes were calculated using the following definition:

$$C_d = A_e/A_g, \tag{1}$$

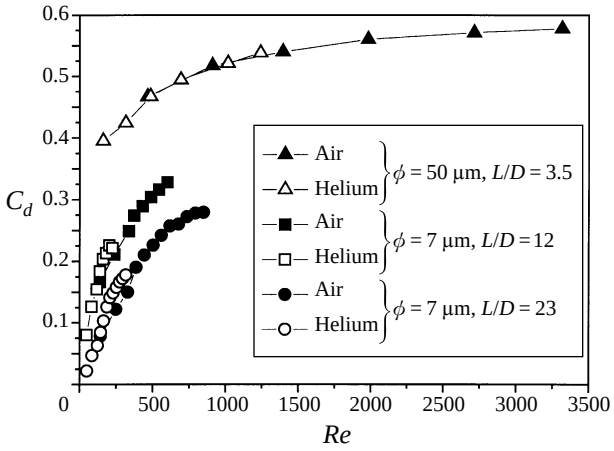

FIGURE 8. Micro-orifice discharge coefficients vs. Reynolds number.

where A_e is the effective flow area in which all the system flow losses are grouped, and A_g is the measured geometric flow area. This relation is derived from the definition of the discharge coefficient as the ratio of the measured flow rate to the ideal isentropic flow rate (Shapiro 1953). The measured flow rate is used to calculate the effective flow area for given stagnation properties and the nozzle pressure ratio using a compressible flow isentropic relationship (Shapiro 1953)

$$A_e = \left(\frac{m_{gas}(R_g T_t)^{1/2}}{P_t Ma(\gamma)^{1/2}}\right)\left(1+\frac{\gamma-1}{2}Ma^2\right)^{(\gamma+1/2(\gamma-1))}, \tag{2}$$

where m_{gas} is the gas mass flow rate, R_g the gas constant, P_t and T_t the upstream stagnation pressure and temperature, $Ma = (2/(\gamma-1)(P/P_t))^{1/2}$ the Mach number and γ the gas specific heat ratio.

Discharge coefficients were calculated for both air and helium gas without liquid flow to the membrane. Figure 8 illustrates that for each membrane the discharge coefficients for both gases correlates with the Reynolds number ($Re = \rho VD/\mu$). For all flow cases with the 7 μm orifice membranes (and the majority of the 50 μm cases), the flow Reynolds number is below the 2300 value for transition to turbulence (Fox & McDonald 1985). The generally low discharge coefficient values indicate that significant flow losses occur in the micro-machined flow orifices. This can be attributed to the loss from both the sharp-edged inlet and exit geometries, frictional losses due to the high L/D values, and possible Knudsen number effects in small passages (Harley *et al.* 1995).

The addition of a liquid methanol film applied to the top surface of the membrane produced a slight increase in C_d values, as shown in figure 9 for the 7 μm membrane with $L/D = 12$. The gas-only data are the averages of three measurements along with the 95% confidence bands ($\pm 4.303\sigma/\sqrt{3}$ (Dixon & Massey 1983)). This trend of increased discharge coefficient when the gas jets interacted with a liquid film was also observed for the 7 μm $L/D = 23$ membrane. This could be due to the reduction in temperature of the droplet generator housing which was observed during operation but was not quantified. A corresponding reduction in gas temperature due to the evaporative cooling of the liquid methanol would lower the dynamic viscosity of a gas while raising its density, thereby increasing the C_d value. All of the effective flow area calculations assumed a constant 20 °C stagnant gas temperature in the gas plenum. The

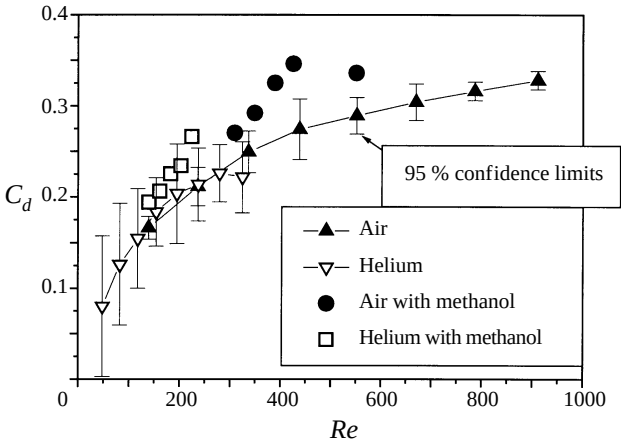

FIGURE 9. $\phi = 7$ μm, $L/D = 12$, membrane discharge coefficients vs. Reynolds number gas flow only and gas with liquid film.

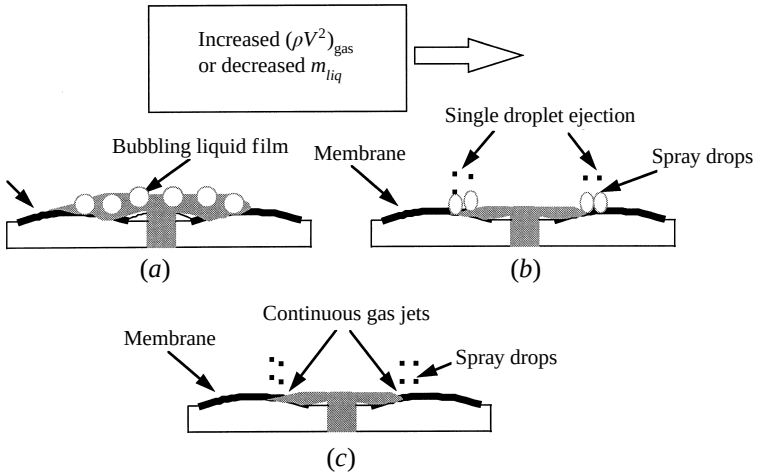

FIGURE 10. Spray regimes: (*a*) bubbling, (*b*) drop eject, (*c*) micro-gas-assisted.

50 μm membrane did not exhibit this sensitivity of the discharge coefficient in the presence of a liquid film, possibly due to the significantly larger C_d values obtained in comparison to those from the 7 μm membranes.

The entrance length prediction for laminar pipe flow (White 1974) was compared to the membrane thickness. The lowest level of gas pressurization in the tests with the 7 μm membranes was 239 kPa and in this case an entrance length exceeding the orifice length was predicted for all cases except when using helium with the $L/D = 23$ membrane. All of the entrance lengths for the 50 μm membranes exceeded the orifice length. Therefore, for the majority of the sprays produced, the discharging gas jets can be characterized as developing, laminar, choked flows.

3.2. *Atomization*

Three distinct droplet production regimes were identified when air and helium were used as the atomization gases and the membranes were exposed to a range of liquid methanol flow rates, as outlined in figure 10. Two of these regimes were observed with the 7 μm membranes: the gas bubbling (figure 10*a*) and the droplet ejection spray

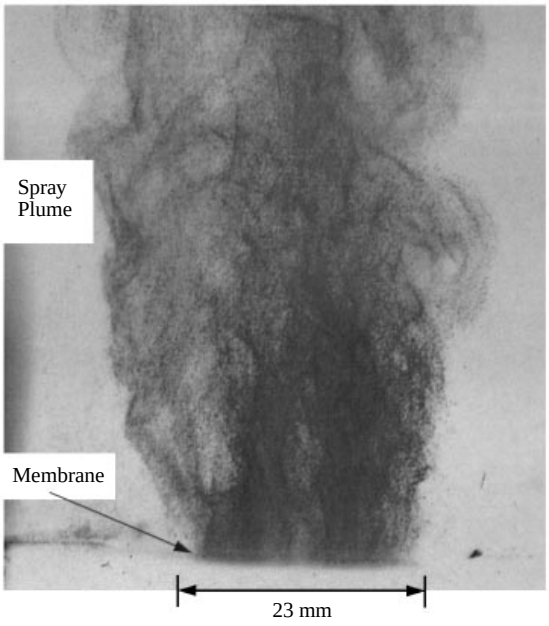

FIGURE 11. Spray plume, $P_{gas} = 239$ kPa, $m_{air} = 0.020$ g s^{-1}, $m_{methanol} = 0.057$ g s^{-1} (ALR = 35.1 %).

regime (figure 10*b*). In the bubbling regime, the injected gas jets form detached bubbles within the liquid layer, similar to pool boiling. The bubbles burst after a period of time at the free surface, as previously discussed (Newitt *et al.* 1954). Very small numbers of minute liquid droplets are produced in this regime, as the majority of the mass does not escape the surface (see figure 1).

Reducing the film thickness or increasing the dynamic pressure of the discharging gas jets produces the spray droplet ejection regime. In this case, a directed spray plume of small-diameter droplets rises above the surface as shown in figure 11 using a 7 μm membrane. This is a steady operating condition in which the liquid film momentarily blocks each discharge orifice exit. This blockage forms a liquid 'cap' which is blown out of the film by the action of the gas jet to form a droplet, as discussed further below.

Figure 12(*a*) displays details of the droplet ejection regime using the 50 μm orifice with helium at a low pressure of 136 kPa. The liquid film above each gas orifice is seen to be inflated and stretched by the discharging gas jet which is trapped by the liquid film. When the liquid surface forces release the liquid cap, a single droplet, approximately 100 μm in diameter for the conditions in figure 12(*a*), was released.

Decreasing the orifice size to 7 μm allows the ejection regime to exist over a wider range of dynamic gas pressures, for both air and helium as the driving gas. Figure 12(*b*) displays a 20 μm droplet being ejected from an extended liquid structure using 377 kPa air as the atomizing gas. As in the 50 μm example (figure 12*a*), the liquid is stretched until the end cap is pinched or blown off. The minimum ratio of atomizing gas-to-liquid flow rate is determined when the transition to the bubbling regime occurs.

The third regime, a micro-gas-assisted spray regime, occurs when the film thickness is reduced or the dynamic gas pressure is increased further. In this mechanism a solid gas jet is maintained in each hole which continuously pierces through the liquid film and entrains liquid droplets and ligaments. The discharging air jet is surrounded by an annular methanol film, as shown in figure 13, with the 50 μm membrane pressurized to

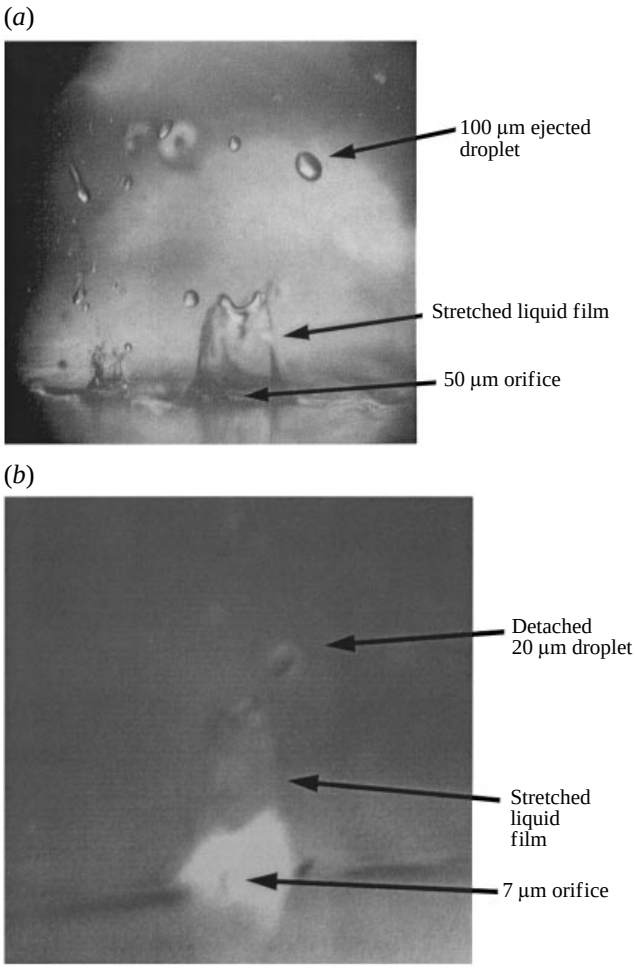

FIGURE 12. Drop ejection regime: (*a*) $\phi = 50$ μm, helium, $P_{gas} = 136$ kPa, methanol; (*b*) $\phi = 7$ μm, air, $P_{gas} = 377$ kPa, methanol. (The white region in the foreground is a reflection.)

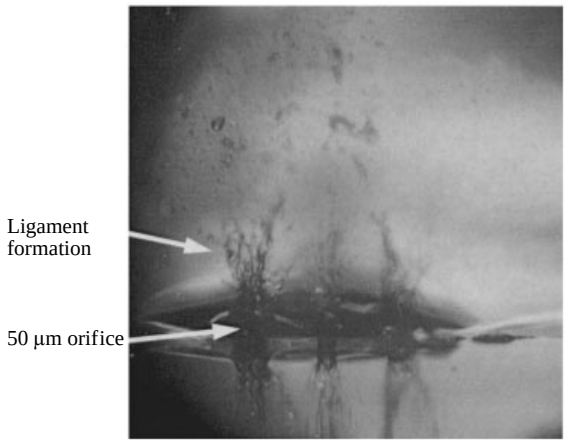

FIGURE 13. Micro-gas-assisted atomization mechanism, air, $P_{gas} = 377$ kPa.

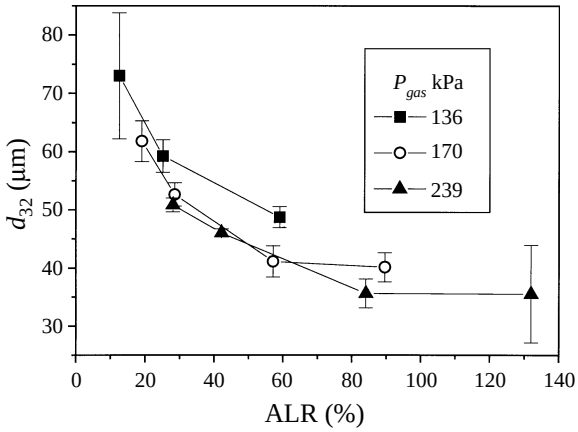

FIGURE 14. SMD vs. ALR, $\phi = 50$ μm, $L = 175$ μm, air and methanol.

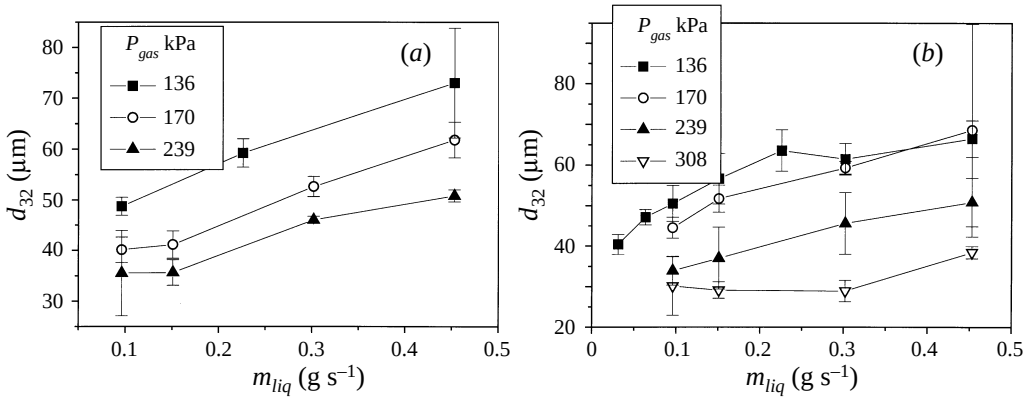

FIGURE 15. SMD vs. m_{liq}, $\phi = 50$ μm, $L = 175$ μm; (*a*) air and methanol, (*b*) helium and methanol.

377 kPa. This regime is similar to that in conventional air-assisted atomizers in which a liquid annulus exits the nozzle. This annulus then fractures into intermediate ligament structures which become unstable and form the spray droplets (Strapper & Samuelson 1990). This process is functionally similar to atomization from a flat liquid sheet (Dombrowski & Johns 1963).

This interpretation of the results is supported by examination of the droplet sizes produced from the 50 μm membrane which displayed two characteristic trends common to gas-assisted atomizers (Lefebvre 1989). First, the spray droplet sizes decreased as the ratio of air-to-liquid (ALR) flow rates (on a mass basis) was increased. Secondly, the droplet sizes decreased as the pressure of the driving gas was elevated. Figure 14 illustrates these trends for the 50 μm diameter orifice membrane, showing SMD vs. air-to-liquid ratio for air and methanol. These trends are also evident when the same SMD data are examined versus the liquid flow rate, as shown in figure 15(*a*). The use of helium as the atomizing gas does not alter the characteristic trends observed for the 50 μm orifice diameter air cases, as shown in figure 15(*b*). In addition, the droplet sizes produced were very similar to those obtained with air as the driving gas, when examined versus liquid flow rate.

All of the droplet sizing tests were performed with the PDPA probe volume located directly above the flow orifices at a distance of 12.7 mm from the membrane. For all

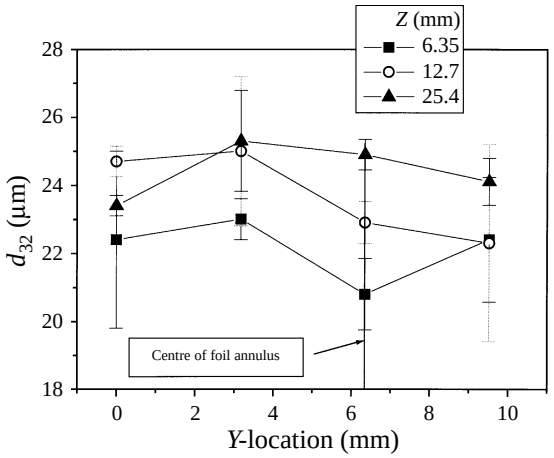

FIGURE 16. SMD vs. radial location, $\phi = 7$ μm, $L/D = 12$, $P_{air} = 239$ kPa, ALR = 46%, methanol.

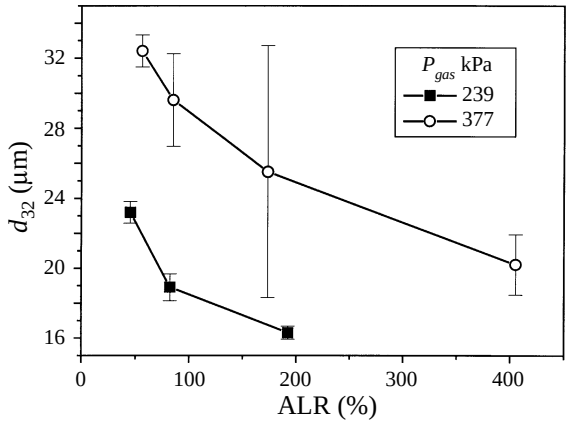

FIGURE 17. SMD vs. ALR, $\phi = 7$ μm, $L/D = 12$, air, methanol, $P_{air} = 239$ and 377 kPa.

of the $\phi = 50$ μm membranes, sporadic groups of large droplets were observed to be propelled in the radial direction across the surface of the membrane as the liquid flow rate was increased. These droplets were not consistently detected by the PDPA device, causing the wider 95% confidence bands at the higher liquid flow rates, as shown in figures 15(*a*) and 15(*b*).

The 7 μm membranes yielded a directed, vertical spray plume, as shown in figure 11, which did not exhibit any evidence of the sporadic ejection of large droplets with radial trajectories observed with the 50 μm sample. Examination of droplet size versus radial location along the membrane, shown in figure 16, indicates that there was less than a 3 μm variance in SMD values across the spray plume above the membrane surface for the three elevations shown.

The 7 μm membranes, operating in the droplet ejection regime, produced several unique atomization characteristics in comparison to the standard gas-assisted atomizer trends noted above when using the 50 μm membrane. Figure 17 reveals that unlike the larger orifice diameter membrane data of figure 14, for a given ALR value, a significant droplet size increase is evident as the gas pressure is elevated from 239 to 377 kPa. These data were acquired using air and methanol at a measurement location 12.7 mm

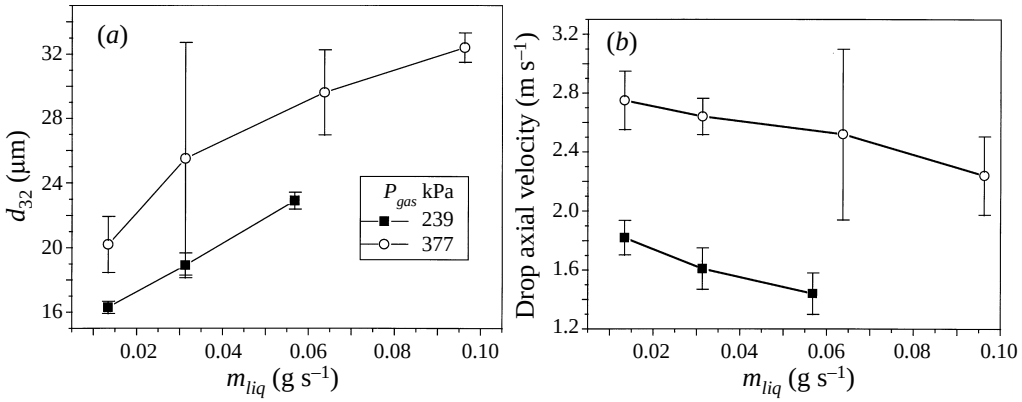

FIGURE 18. (*a*) SMD vs. m_{liq}, and (*b*) Drop axial velocity vs. m_{liq}: $\phi = 7$ μm, $L/D = 12$, air, $P_{air} = 239$ and 377 kPa and (*a*) ethanol, (*b*) methanol.

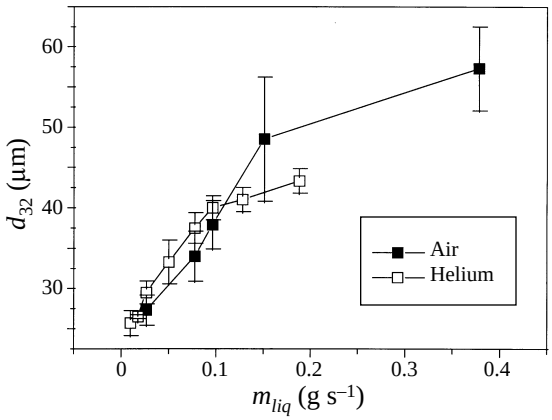

FIGURE 19. SMD vs. m_{liq}, $\phi = 7$ μm, $L = 160$ μm, $P_{gas} = 515$ kPa, air and helium, methanol.

above the surface of the $L/D = 12$ membrane. The minimum ALR corresponds to the maximum liquid flow rate possible for a given gas pressure, while still operating in the drop ejection mode (i.e. before the bubbling regime was initiated).

The difference between the droplet sizes for the two gas pressures is minimized when the size data are examined as a function of liquid flow rate, as shown in figure 18(*a*). A slight increase in droplet size is still observed at the higher gas pressure but variation in droplet size appears to be predominantly controlled by the liquid rate to the membrane, not the gas plenum pressure.

While the droplet size in the ejection regime was not a strong function of gas pressure, the droplet velocity was found to be directly influenced by gas pressure. Figure 18(*b*) illustrates the average measured vertical velocity for the same data as shown in figure 18(*c*). Increasing the gas pressure differential across the membrane by a factor of two raised the average droplet velocity by approximately 50 %.

Increasing the membrane thickness to $L/D = 23$ allowed the maximum gas pressure to be raised to 515 kPa, compared to 377 kPa for the thinner ($L/D = 12$) membrane. Figure 19 displays the corresponding SMD versus liquid flow rate data using both air and helium as the atomizing gas to create methanol droplets. For liquid flow rates below 0.1 g s^{-1} the two 7 μm membranes were found to yield similar droplet sizes (compare to figure 18*a*). The ability to operate at higher gas pressures with the thicker

membrane delayed the transition to the bubbling mode, which allowed a larger maximum liquid flow rate to be used (e.g. up to 0.38 g s^{-1}). The droplet sizes measured over the extended flow range followed the trend established with the $L/D = 12$ membrane and increased with liquid flow.

The limited effect of atomizing gas type on droplet size is also shown in figure 19. For a given liquid flow (i.e. below the transition to the bubbling regime) both air and helium produced similar droplet sizes with the 7 μm membranes, despite the lower gas-to-liquid mass ratio and greater sound speed of helium.

4. Discussion

The bubbling regime of atomization (figure 10*a*), while producing droplet populations with SMD values below 50 μm, requires excessive gas flow since the majority of liquid mass is re-captured by the free surface as the drops fall back under the influence of gravity (see figure 1). When the membranes are operated in this mode, the supplied gas forms distinct bubbles at the top surface which have detached from the gas injection orifice. Atomization occurs when the top of the liquid membrane has sufficiently thinned and subsequently ruptures. Droplet production is loosely coupled to gas orifice size through the bubble size (Newitt *et al.* 1954) via the buoyancy/surface tension force balance (Wallis 1979). However, the droplet creation process is essentially de-coupled from the gas jet dynamics at the orifice exit. A significant increase in the gas dynamic pressure at the orifice exit, or decrease in liquid film thickness, creates the micro-gas-assisted spray regime (figure 10*c*) in which the droplet creation is coupled directly to a specific orifice. The gas jet pierces through the liquid film and thus dictates the conditions, namely length scale and relative velocity, at which the droplets are formed. This mechanism followed established trends of gas-assisted devices in which increases in the gas pressure and ALR reduce the droplet size. The micro-gas-assisted mechanism can be transformed into the bubbling regime if the liquid film thickness is sufficiently large such that the gas jet is dissipated within the liquid, forming distinct bubbles. In between these two mechanisms exists a third operating regime, made possible by controlling the gas jet and liquid interface on the micron size scale, yielding controlled transient production of small droplets without continuously piercing the liquid film.

The droplet ejection regime (figure 10*b*) displayed the characteristics of efficient, small droplet production and the inherent ability to de-couple the ejected droplet's size from its velocity. These unique and desirable traits justify closer examination of this new atomization mechanism for a variety of applications.

The high-speed video camera allowed observation of the transient droplet production mechanism and the droplet ejection sequence (shown in figure 12) is summarized qualitatively in figure 20. Initially, figure 20(*a*), a liquid film covers the exit of the flow orifice. Due to impingement by the gas jet the liquid film becomes stretched, as shown in figure 20(*b*). An extended hollow liquid structure is formed, as shown in figure 20(*c*) as the liquid directly over the orifice is elevated above the foil surface. The rapid action of the gas jet combined with the small radius of curvature of the resulting liquid cap due to the tiny gas jet causes a single droplet to be pinched off at the tip of the elevated liquid structure, as shown in figure 20(*d*). The curvature of the liquid cap maintains the thick film at the tip of the elevated structure, preventing the breakthrough of the gas jet and the subsequent transition to the micro-gas-assisted mode. The stretching of the liquid film by the action of the gas jet causes the thinning of the connecting annulus. This reduces the flow area available for liquid from the cap to escape back into the

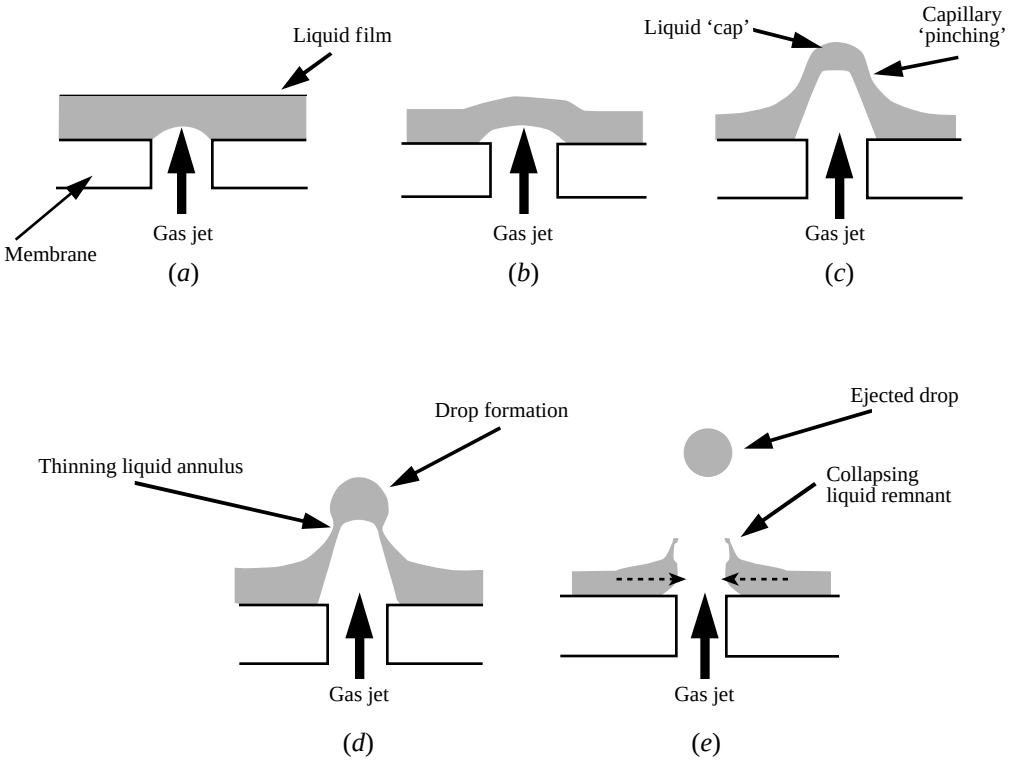

FIGURE 20. Drop ejection mechanism.

main body of liquid in the film. The reduced flow area limits the drainage of liquid from the cap, trapping it on top of the gas jet. At the point that the connecting annulus ruptures, a single droplet is ejected and a solid gas jet momentarily pierces through the liquid film as depicted in figure 20(*e*). The recoil inertia of the collapsing liquid structure overwhelms the static gas pressure at the jet exit and new liquid rushes inwards to block the orifice exit and the process is repeated.

For the 7 μm diameter orifices the time between droplet ejection events was determined from the high-speed movies to be in the range 100–400 μs. The time required for the film to be stretched and to eject a droplet varied from less than 25 μs (the temporal resolution of the movies) to approximately 100 μs. Based on these numbers it is estimated that a continuous gas jet flows through the orifice for as much as 75% of the total cycle time. This explains why the discharge coefficients of figure 9 were similar for the membrane with and without the liquid film.

In the above scenario the droplet size can be seen to be related to the thickness of the liquid film. This is also consistent with the data which showed that the droplet size increased with the liquid flow rate (see figure 18*a*). The droplet is essentially 'punched' out of the liquid film and therefore mass conservation yields the following relation:

$$\rho_{liq}\frac{\pi \mathrm{d}_{drop}^3}{6} = \rho_{liq}\,\pi\phi^2 t_F, \tag{3}$$

where t_F is the idealized initial liquid film thickness, as illustrated in figure 21. Therefore the droplet size $\propto t_F^{(1/3)}$. In practice t_F is a function of the location of the orifice on the membrane (due to the deflection of the membrane which influences the local film thickness) and the liquid flow rate. Examination of the SMD versus liquid

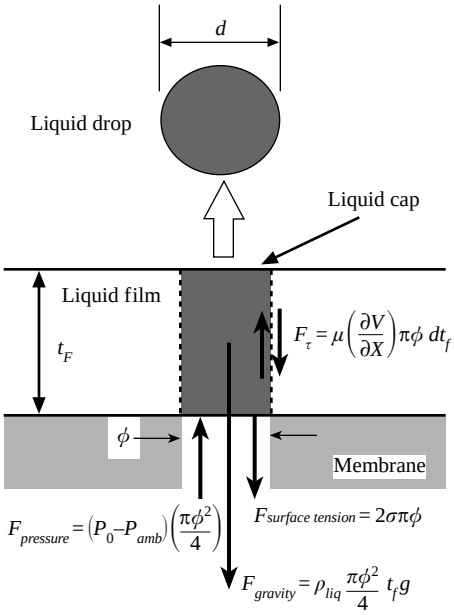

FIGURE 21. Force balance.

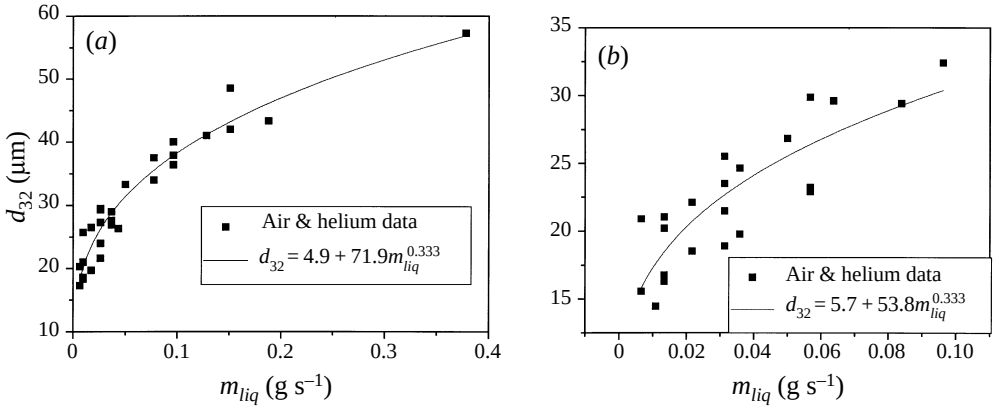

FIGURE 22. SMD vs. liquid flow rate, curve fit to 1/3 power: $\phi = 7$ μm, (*a*) $L/D = 23$, (*b*) $L/D = 12$.

flow rate results for the 7 μm membranes operating in the droplet ejection regime supports this analysis. Figure 22(*a*) displays the SMD values obtained with the thick membrane ($L/D = 23$) acquired using 239, 377 and 515 kPa gas pressures for both air and helium. The solid line provides a satisfactory curve fit to the data with the flow rate raised to the 1/3 power. A similar relation is displayed in figure 22(*b*) for the thin membrane ($L/D = 12$), with a mean-square error of 2.1 μm for both figures.

The $L/D = 12$ membrane was able to operate in the droplet ejection regime over the majority of its surface even when the extreme radial locations had transitioned into the bubbling regime. Therefore an upper limit on the film thickness of 160 μm and 200 μm for the 239 and 377 kPa gas pressures, respectively, can be empirically established. When the liquid film thickness exceeded these values over an orifice, free-floating gas bubbles were formed and the droplet ejection mechanism ceased. It is interesting to

note that the predicted bubble size using a buoyancy/surface tension force balance (using a 7 μm diameter cylindrical neck of an attached air bubble in methanol) yields a maximum bubble diameter of 500 μm (Wallis 1979). Therefore it can be concluded that the transition to the bubbling regime is not solely based upon buoyancy but is augmented by the cyclic oscillation of the surface standing waves which are driven by the collapse of the liquid structure from a neighbouring orifice. The interaction of these waves would act to vary the film thickness, producing a range of droplet sizes across the membrane surface and prematurely halting the droplet ejection regime.

A static force balance was considered on a control volume encompassing the cylinder-shaped liquid cap, shown in figure 21. The pressure difference across the liquid film is related to the gravity force of the liquid over the orifice exit, the viscous shear within the liquid and the surface tension forces at both the top and bottom surfaces of the control volume which act to maintain film integrity.

In order to analyse the movement of the liquid cap the force balance can be written as

$$M\frac{\mathrm{d}V}{\mathrm{d}t} = F_p - F_\tau - F_s - F_g, \tag{4}$$

where $m = \rho\pi\phi^2 t_F/4$ is the mass of fluid being accelerated and V is the instantaneous vertical velocity of the cap (assumed to be uniform within the fluid cap). The pressure force is estimated as $F_p = (P_r - P_{amb})\pi\phi^2/4$, where P_r is the gas pressure under the cap. This is assumed to be related to the reservoir driving gas pressure below the membrane, P_o, through the impulsive piston withdrawal result $P_r/P_o = (1 - \frac{1}{2}(\gamma-1)\,V/c_0)^{2\gamma/\gamma-1}$, where c_o is the sound speed in the gas. The viscous shear force at the edge of the control volume is approximated as $F_\tau = \mu\,\mathrm{d}V/\mathrm{d}x\,\pi\phi t_F = c_1\mu 2V\pi t_F$, where C_1 is a constant of order unity. The surface tension force which restrains the cap is estimated to be $F_s = C_2\sigma\pi\sigma$ (with $C_2 \approx O(1)$) and, finally, the body force is $F_g = Mg$. Order of magnitude estimates show that the viscous force is a dominant term. In this case, with the assumption that $V \quad c_o$, it can be shown that the cap's escape velocity, i.e. $V(t \to \infty)$, is

$$V = (P_o - P_{amb})\,\phi^2/8\mu t_F. \tag{5}$$

As an example, using (3) with an assumed drop size of 15 μm, a driving gas pressure $P_0 = 200$ kPa and $\phi = 7$ μm, gives $V \approx 2\ \mathrm{m\ s^{-1}}$. This estimate agrees well with the magnitude of the measured drop velocity (see figure 18*b*). The characteristic time to accelerate the cap to its escape velocity (the drop formation time) is estimated to be $\approx \phi^2/8\nu$ which is about 6 μs for the example case. This is also a reasonable estimate, based on analyses of the high-speed movie frames.

This first-order analysis indicates that the viscous shear controls the upward acceleration of the liquid cap. The rapid acceleration of the liquid above the orifice is essential to prevent the draining of the liquid from the cap back into the film, thus thinning the portion of the cap directly impinged by the gas jet. Film rupture at this location yields a solid gas jet discharging through the liquid film producing the micro-gas-assisted regime. Maintaining the liquid in the cap region and rupturing the film around the liquid cap is a critical requirement for the droplet ejection mechanism.

5. Summary

Advancements in micro-machining technology are providing new opportunities for the study of micro-fluid dynamics in which surface forces effectively compete with body forces. This paper reviews the discovery of a unique liquid atomization mechanism,

made possible by the use of deep X-ray lithography/electrodeposition processes. In the present application, a liquid film is disrupted by thousands of small-diameter gas jets from a micro-machined membrane.

Distinct differences in the fluid mechanics of the gas/liquid interaction between 7 and 50 μm gas flow orifices were observed. The performance trends of the larger diameter (50 μm) orifices mimicked those seen in conventional gas-assisted mechanisms of liquid sheet breakup, but on a much smaller scale. The liquid sheet formed at the exit of each orifice was segmented into ligaments by the high relative gas/liquid velocity which energized surface instabilities. These ligaments subsequently form droplets with their final size dependent upon the ligament diameter and the relative gas/ligament velocity.

The new droplet ejection regime observed in this work when using the 7 μm diameter orifice membranes bypassed the ligament formation stage in such a way as to directly extract distinct liquid droplets on the order of 20 μm in diameter from the liquid film. By inflating the film prior to its rupture, a portion of the gas flow energy is directly used to thin the liquid film. This is inherently more efficient than relying on a high relative gas/liquid velocity because all of the gas flow energy during the inflation portion of the cycle contributes to the liquid stretching, not just through a shear gas flow at a liquid surface, as in the conventional gas-assisted atomizer. The thinning acts on the connecting film around an isolated liquid fragment and ruptures it prior to the gas jet piercing the liquid film, ejecting the liquid 'cap'.

The interaction of a liquid film with a field of 7 μm diameter micro-gas jets produces significantly smaller droplet sizes with less energy input when compared to the flow requirements of the 50 μm diameter jets. The droplet sizes produced from the present droplet ejection mechanism have been shown to follow the relation, diameter $\propto$ film thickness$^{(1/3)}$, and the droplet size is essentially independent of the driving gas pressure. The droplet velocity is related to the driving pressure, the film thickness, the nozzle hole diameter and the fluid viscosity. As a result the droplet size and velocity are de-coupled and can be controlled independently. These characteristics are extremely desirable in applications where rapid and controlled two-phase gas and liquid mixing is a requirement.

The authors acknowledge the assistance of the staff of the Center for X-ray Lithography at the UW-Madison, especially Dr Greg Wells and Dr Matt Loudon for their invaluable assistance in the construction of the orifice membranes. In addition, the assistance of Mr Paul Tennison and Mr Calvin Hung with the droplet sizing experiments is appreciated. The authors also acknowledge the funding from the Army Research Office (ARO), Caterpillar Inc., and S.C. Johnson Wax.

REFERENCES

Boulton-Stone, J. M. & Blake, J. R. 1993 Gas Bubbles bursting at a free surface. *J. Fluid Mech.* **254**, 437.

Dixon, W. J. & Massey, F. J. 1983 *Introduction to Statistical Analysis*. McGraw-Hill.

Dombrowski, N. & Johns, W. R. 1963 The aerodynamic instability and disintegration of viscous liquid sheets. *Chem. Engng Sci.* **18**, 203.

Fox, R. W. & McDonald, A. T. 1985 *Introduction to Fluid Mechanics*. John Wiley & Sons.

Frasier, R. P., Dombrowski, N. & Routley, J. H. 1963 The atomization of a liquid sheet by an impinging air stream. *Chem. Engng Sci.* **18**, 339.

Harley, J. C., Huang, Y., Bau, H. H. & Zemel, J. N. 1995 Gas flow in micro-channels. *J. Fluid Mech.* **284**, 257.

Lefebvre, A. H. 1989 *Atomization and Sprays*, Hemisphere.

Newitt, D. M., Dombrowski, N. & Knelman, F. H. 1954 Liquid Entrainment 1. The mechanism of drop formation from gas or vapour bubbles. *Trans. Inst. Chem. Engrs* **32**, 244.

Shapiro, A. H. 1953 *The Dynamics and Thermodynamics of Compressible Fluid Flow*. Wiley.

Snyder, H. E. 1997 Efficient Liquid Atomization using gas flows and novel micro-machining techniques. PhD thesis, University of Wisconsin-Madison.

Strapper, B. E. & Samuelsen, G. S. 1990 An experimental study of the breakup of a two-dimensional sheet in the presence of co-flow air shear. *AIAA Paper* 90-0461.

Wallis, G. B. 1979 *One-Dimensional Two Phase Flow*. McGraw-Hill.

White, F. M. 1974 *Viscous Fluid Flow*. McGraw-Hill.